

Open cluster survival within the solar circle: Teutsch 145 and Teutsch 146*

C. Bonatto¹, S. Ortolani², B. Barbuy³ and E. Bica¹

¹ *Departamento de Astronomia, Universidade Federal do Rio Grande do Sul, Av. Bento Gonçalves 9500, Porto Alegre 91501-970, RS, Brazil*

² *Dipartimento di Astronomia, Vicolo dell'Osservatorio 5, I-35122 Padova, Italy*

³ *Departamento de Astronomia, Universidade de São Paulo, Rua do Matão 1226, São Paulo 05508-900, SP, Brazil*

16 December 2018

ABSTRACT

Teutsch 145 and Teutsch 146 are shown to be open clusters (OCs) orbiting well inside the Solar circle, a region where several dynamical processes combine to disrupt most OCs on a time-scale of a few 10^8 yrs. BVI photometry from the GALILEO telescope is used to investigate the nature and derive the fundamental and structural parameters of the optically faint and poorly-known OCs Teutsch 145 and 146. These parameters are computed by means of field-star decontaminated colour-magnitude diagrams (CMDs) and stellar radial density profiles (RDPs). Cluster mass estimates are made based on the intrinsic mass functions (MFs). We derive the ages 200_{-50}^{+100} Myr and 400 ± 100 Myr, and the distances from the Sun $d_{\odot} = 2.7 \pm 0.3$ kpc and $d_{\odot} = 3.8 \pm 0.2$ kpc, respectively for Teutsch 145 and 146. Their integrated apparent and absolute magnitudes are $m_V \approx 12.4$, $m_V \approx 13.3$, $M_V \approx -5.6$ and $M_V \approx -5.3$. The MFs (detected for stars with $m \gtrsim 1 M_{\odot}$) have slopes similar to Salpeter's IMF. Extrapolated to the H-burning limit, the MFs would produce total stellar masses of $\sim 1400 M_{\odot}$, typical of relatively massive OCs. Both OCs are located deep into the inner Galaxy and close to the Crux-Scutum arm. Since cluster-disruption processes are important, their primordial masses must have been higher than the present-day values. The conspicuous stellar density excess observed in the innermost bin of both RDPs might reflect the dynamical effects induced by a few 10^8 yrs of external tidal stress.

Key words: (*Galaxy*) open clusters and associations; *Galaxy*: structure

1 INTRODUCTION

Regions interior to the Solar circle represent a harsh environment to the long-term survival of open clusters (OCs). The low-mass ones in particular, dissolve into the field in less than ≈ 1 Gyr (e.g. Friel 1995; Bonatto & Bica 2007b).

Theoretical and N-body predictions (e.g. Spitzer 1958; Lamers & Gieles 2006; Baumgardt & Makino 2003; Goodwin & Bastian 2006; Khalisi, Amaro-Seoane & Spurzem 2007), coupled to observational evidence (e.g. van den Bergh 1957; Oort 1958; von Hoerner 1958; Piskunov et al. 2007) consistently indicate that the disruption-time scale (t_{dis}) near the Solar circle is shorter than ~ 1 Gyr and depends on cluster mass as $t_{\text{dis}} \sim M^{0.62}$ (Lamers & Gieles 2006). Thus,

$75 \lesssim t_{\text{dis}}(\text{Myr}) \lesssim 300$ should be expected for clusters with an initial mass within $10^2 - 10^3 M_{\odot}$. Besides, disruption processes are more effective for the more centrally located and lower-mass OCs (see Bonatto & Bica 2007b for a review on these effects).

It is in this context that the discovery and characterization of new OCs towards the inner Galactic regions play an important role. Here we establish the nature and derive astrophysical parameters of the poorly-studied, faint OCs Teutsch 145 and 146. Both clusters were discovered by Phillip Teutsch in a systematic survey of several Milky Way fields near the Galactic plane using red, blue, and infrared First and Second Generation DSS images downloaded from the ESO Online Digitized Sky Survey (Kronberger et al. 2006). We are dealing with 1st Galactic Quadrant clusters, which makes them particularly suitable to explore dynamical cluster properties within the Solar circle.

Algorithms designed to deal with field-star contamination in densely populated fields, together with other tools to study colour-magnitude diagrams (CMDs) and stellar radial density profiles (RDPs) have been developed by our group

* Based on observations made with the Italian Telescopio Nazionale GALILEO (TNG) operated on the island of La Palma, by the Fundación Galileo Galilei of INAF (Istituto Nazionale di Astrofisica) at the Spanish Observatorio del Roque de los Muchachos of the Instituto de Astrofísica de Canarias

Table 1. Position and angular size

Cluster	$\alpha(2000)$ (hms)	$\delta(2000)$ ($^{\circ}$ $'$ $''$)	ℓ ($^{\circ}$)	b ($^{\circ}$)	D ($'$)
(1)	(2)	(3)	(4)	(5)	(6)
Teutsch 145	18:42:29	-05:15:12	27.24	-0.41	1.9
Teutsch 146	18:51:34	+00:11:10	33.11	+0.06	1.6

Table Notes. Col. 6: optical diameter measured in the DSS images.

in previous 2MASS¹ studies (e.g. Bica, Bonatto & Camargo 2008; Bonatto & Bica 2008b; Bonatto & Bica 2009a). In the near future, VISTA² together with other surveys with large telescopes, will deepen by about 4 magnitudes the presently-available near infrared photometry in a large area throughout the Galactic plane. The new - and deeper - photometry will probably require specific algorithms to be analysed. Thus, besides the more direct goal of deriving parameters of two interesting objects, in the present work we apply our analytical tools to the optical data of the two faint open clusters, Teutsch 145 and 146, obtained with the 3.58m GALILEO telescope (TNG)³.

Since they are located in the 1st Quadrant (with the associated enhanced disruption rates), the heavy field contamination should be properly taken into account for the intrinsic properties to be assessed. In this context, our main goal in this work is to determine whether such clusters can be characterised as typical OCs or if they present signs of dissolution. In addition, we will derive their fundamental and structural parameters, most of these for the first time.

This paper is organised as follows. In Sect. 2 we provide details on the observations, photometric calibrations and reductions. In Sect. 3 we build the colour-magnitude diagrams, discuss the field decontamination and derive the fundamental parameters. In Sect. 4 we derive structural parameters. In Sect. 5 we estimate cluster mass and build the mass functions. In Sect. 6 we discuss the parameters of both OCs. Concluding remarks are given in Sect. 7.

2 OBSERVATIONS

Teutsch 145 and 146 were observed in 2008 June with the 3.58m GALILEO telescope (TNG) at La Palma, equipped with the Dolores spectrograph focal reducer. A EEV 4260 CCD detector with 2048×2048 pixels, of pixel size 13 μ m was used. A pixel corresponds to 0.252'' on the sky, and the full field of the camera is 8.6' × 8.6'. Calibration and reductions are described in detail in Ortolani et al. (2009)

For reddening transformations we use the relations $A_V = 3.1E(B - V)$, $E(V - I) = 1.25E(B - V)$, $A_I = 1.95E(B - V)$, and $A_B = 1.322A_V$, taken from Schlegel, Finkbeiner & Davis (1998), which are based on the

¹ The Two Micron All Sky Survey, All Sky data release (Krutskie et al. 1997) - <http://www.ipac.caltech.edu/2mass/releases/allsky/>

² <http://www.vista.ac.uk/>

³ <http://www.tng.iac.es/>

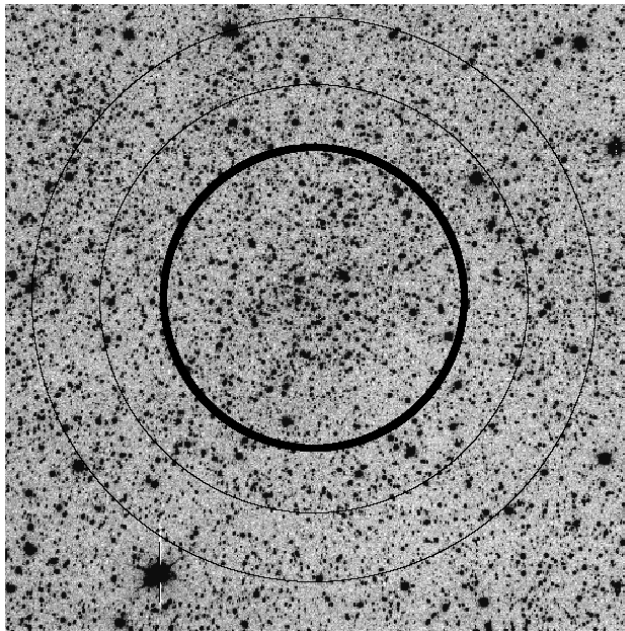


Figure 1. Full-frame ($\approx 8.5' \times 8.5'$), 10sec I band image of Teutsch 145. Extractions corresponding to the cluster ($R \approx 1.8'$) and comparison field ($2.5' \lesssim R \lesssim 3.4'$) are shown by the inner and outer rings, respectively.

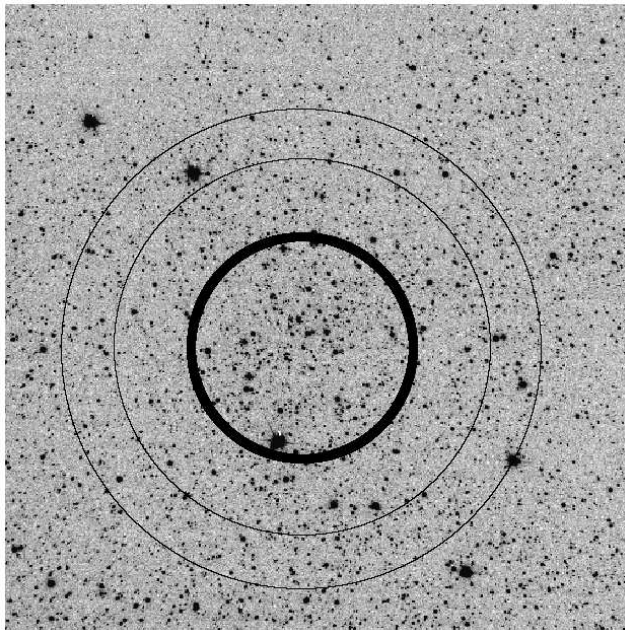


Figure 2. Same as Fig. 1 for Teutsch 146. Cluster and comparison field extractions are $R \approx 1.5'$ and $2.3' \lesssim R \lesssim 2.9'$, respectively.

extinction curves of Cardelli, Clayton & Mathis (1989) and O'Donnell (1994). We remark that the individual values of absorption and reddening in front of the clusters are determined from the CMD fitting (Sect. 3.2).

In Figs. 1 and 2 we show 10 sec I images of both objects and surroundings. We also indicate the regions where most of the cluster's stellar content are located, together with the respective comparison fields.

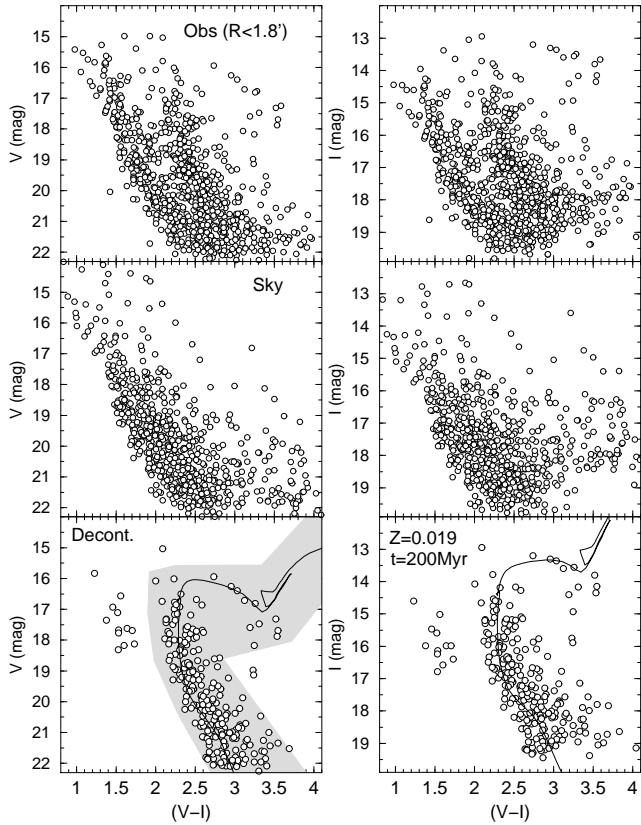


Figure 3. V vs. $(V - I)$ and I vs. $(V - I)$ CMDs of Teutsch 145. Top panels: observed photometry extracted from $R < 1.8'$. Middle: equal-area comparison field extracted from $2.9' \lesssim R \lesssim 3.4'$. Bottom: decontaminated CMDs, including the *best-fit* isochrone solution. The colour-magnitude filter (shaded polygon) is shown in the bottom-left panel.

3 COLOUR-MAGNITUDE DIAGRAMS

CMDs involving V and I of Teutsch 145 and 146 are shown in Figs. 3 and 4, respectively. Based on the structural analysis (Sect. 4), we consider in the top panels the extraction that contains most of each cluster’s stars. When compared with the CMDs extracted from the equal-area comparison field (middle panels), features typical of evolved OCs emerge from the rather heavy disk and bulge contamination: a relatively tight and well-populated main sequence (MS) together with a few giant stars.

CMDs built with the additional B photometry of Teutsch 145 (Fig. 5) consistently present the same morphology as that implied by Fig. 3. However, the important stellar contamination (middle panels) has to be subtracted before proceeding to a more objective interpretation of the CMDs.

3.1 Field decontamination

As illustrated by the CMDs of Teutsch 145 and 146 (Figs. 3-5), field-stars are an important component in CMDs of clusters projected onto rich fields, especially near the disk and bulge. In this paper we work with an algorithm based on the three-dimensional decontamination routine designed for the wide-field 2MASS photometry (Bonatto & Bica 2007a; Bica, Bonatto & Camargo

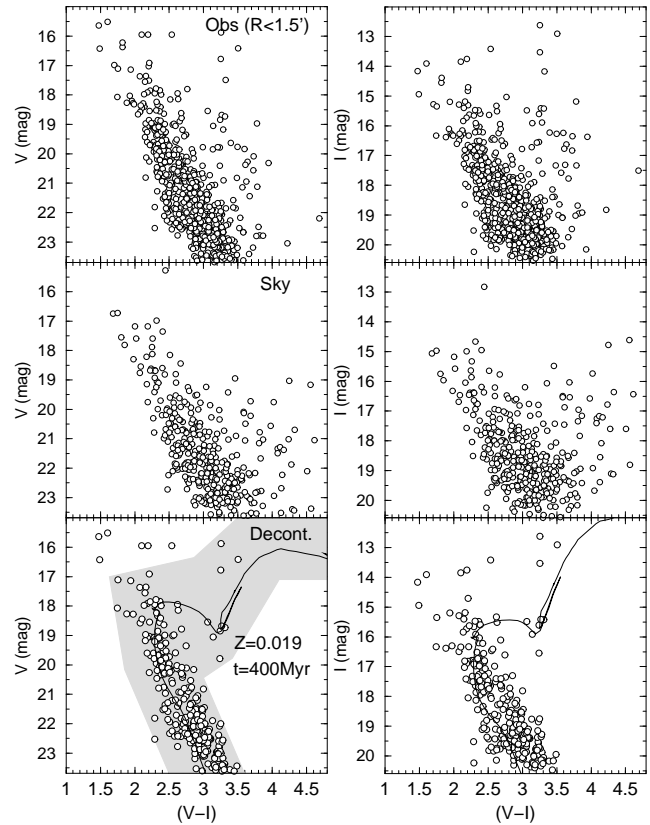


Figure 4. Similar to Fig. 3 for the $R < 1.5'$ extraction of Teutsch 146. Comparison field extracted from $2.5' \lesssim R \lesssim 2.9'$.

2008; Bica & Bonatto 2008). The original algorithm was adapted to deal with photometry obtained with a large telescope and a single colour. For clarity, we recall the basic procedures. The algorithm divides the magnitude and colour ranges into a grid of CMD cells. For a given cluster extraction and comparison field, it estimates the relative number densities of probable field and cluster stars present in each cell. The estimated number of field stars is subsequently subtracted from each cell. Reference cell dimensions are $\Delta \text{mag} = 1.0$ and $\Delta \text{colour} = 0.2$. In addition, we minimise spurious results by means of several runs of the decontamination procedure, with different input parameters. Here, different cell sizes are considered, with Δmag and Δcolour taken as 0.5, 1.0 and 2.0 times the reference values. Also, the cell grid is shifted by $-1/3$, 0 and $+1/3$ of the respective cell size in both the colour and magnitude axes. Taking together all the grid/cell size setups, we are left with 81 different and independent decontamination combinations. Stars are ranked according to the number of times they survive each run. Finally, only the highest ranked stars are considered as cluster members and transposed to the respective decontaminated CMD.

Since the GALILEO field is somewhat limited, covering about $8.5' \times 8.5'$, we take as comparison field the rings within $2.5' \lesssim R \lesssim 3.4'$ and $2.3' \lesssim R \lesssim 2.9'$, respectively for Teutsch 145 and 146. This geometrical setup (Figs. 1 and 2) prevents border effects and minimises the oversubtraction of member stars at the cluster’s outskirts. Indeed, the num-

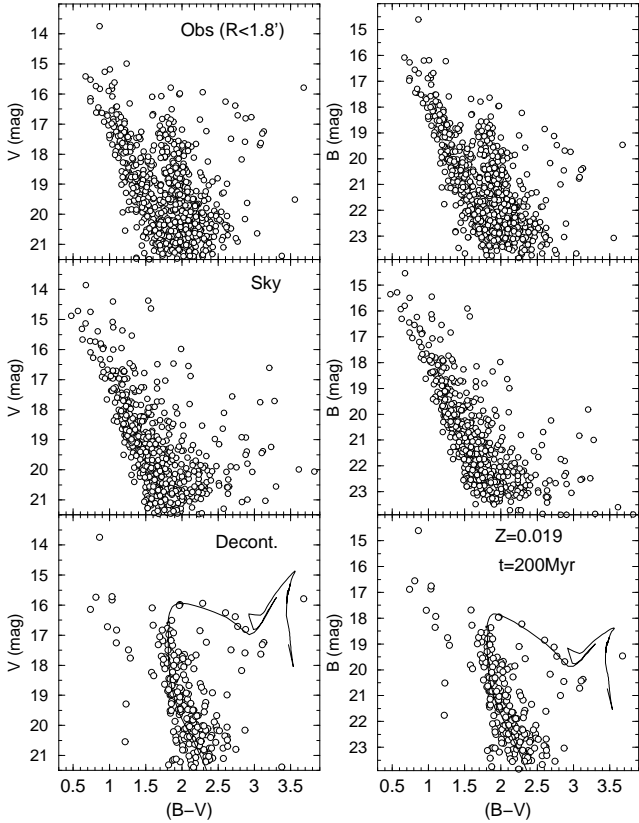


Figure 5. Same as Fig. 3 for the V vs. $(B-V)$ and B vs. $(B-V)$ CMDs of Teutsch 145.

ber density of stars in the comparison fields corresponds to about 1/4 that in the central parts (Fig. 7).

The decontaminated CMDs are shown in the bottom panels of Figs. 3 to 5. As expected, essentially all contamination is removed, leaving stellar sequences typical of reddened and evolved OCs. The decontaminated CMDs also show some scatter that, in the bright CMD sequences, may occur from low-number statistics and, consequently decontamination inefficiency (this issue is thoroughly discussed in Bonatto & Bica 2007a). However, much of the scatter among giants is due to binarism, as detected from proper motions and radial velocity variations (e.g. Hole et al. 2009). In the blue sequences, blue stragglers and binarism in general are important sources of scatter (e.g. Geller et al. 2009). As discussed in Bonatto & Bica (2007a), differential reddening is also a potential source of reddening. However, since (i) the sampled regions are relatively small ($\lesssim 3.5'$), (ii) the foreground absorption is moderate ($A_V \lesssim 6$ mag) in both cases (Sect. 3.2), (iii) the distribution of stars in the I images (Figs. 1 and 2) is rather uniform and, (iv) the cell dimensions used in the decontamination algorithm are wide enough to minimise differential reddening effects, the differential reddening is not expected to be a major source of scatter in the CMDs of Teutsch 145 and 146. The similar decontaminated CMD morphologies indicate comparable ages for both objects.

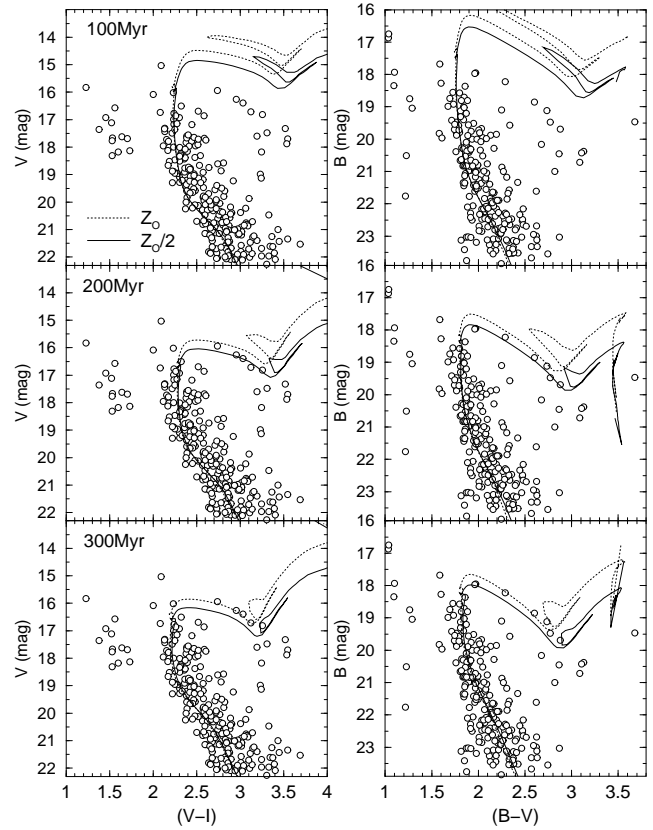


Figure 6. Age and metallicity determination for Teutsch 145.

3.2 Fundamental parameters

We base the fundamental parameter derivation on the field-decontaminated CMD morphologies (Figs. 3-5), using as a constraint the different combinations of magnitudes and colours. Fits with Padova isochrones (Girardi et al. 2002) are made *by eye*, taking the MS and giant stars as constraint. The adopted results are shown in Figs. 3 to 5 (bottom panels) and discussed below.

Teutsch 145: At first sight, the decontaminated features denote an OC a few 10^8 yrs old and nearly solar metallicity. Thus, we search for solutions with isochrones with the ages 100, 200 and 300 Myr, of solar and half solar metallicities. This age/metallicity search is illustrated in Fig. 6, where we use the decontaminated $R = 1.8'$ extraction and the V vs. $(V-I)$ and B vs. $(B-V)$ CMDs. We require that all solutions provide a similar representation of the MS, the more statistically significant CMD feature.

Clearly, Teutsch 145 is older than 100 Myr (top panels) but not much older than 300 Myr (bottom panels). Besides, the solar metallicity isochrone appears to produce the best fit for the best age solution, 200 Myr (middle panels). Thus, taking into account the above range of ages and metallicities, we found that the best solution corresponds to the age 200^{+100}_{-50} Myr and solar metallicity, although lower metallicity values cannot be ruled out.

With the adopted (200 Myr) isochrone solution, the fundamental parameters of Teutsch 145 are the reddening $E(V-I) = 2.37 \pm 0.02$, which converts (Sect. 2) to $E(B-V) = 1.90 \pm 0.02$, a total-to-selective absorption

$A_V = 5.88 \pm 0.06$, the observed and absolute distance moduli $(m - M)_V = 18.0 \pm 0.2$ and $(m - M)_O = 12.12 \pm 0.21$, respectively, and the distance from the Sun $d_\odot = 2.7 \pm 0.3$ kpc. We adopt $R_\odot = 7.2 \pm 0.3$ kpc (Bica et al. 2006) as the Sun's distance to the Galactic centre to compute Galactocentric distances⁴. For $R_\odot = 7.2$ kpc, the Galactocentric distance of Teutsch 145 is $R_{GC} = 5.0 \pm 0.2$ kpc, which puts it ≈ 2.2 kpc inside the Solar circle. This solution is shown in Figs. 3 and 5.

The above fundamental parameters are used to compute integrated magnitudes and colours, for the stars within $R = 1.8'$ isolated by the colour-magnitude filter (Sect. 4). The integrated apparent magnitudes are $m_V \approx 12.4$ and $m_I \approx 9.8$, the reddening-corrected colour is $(V - I) = +0.40 \pm 0.03$, and the absolute magnitudes are $M_V = -5.6 \pm 0.1$ and $M_I = -6.0 \pm 0.1$. Compared to the set of OCs analysed by Lata et al. (2002), Teutsch 145 is intrinsically somewhat brighter than the mean value of the distribution.

Teutsch 146: A similar approach is applied to derive the fundamental parameters of Teutsch 146. Given the similarities with the CMD of Teutsch 145, uncertainties in age and metallicity of the same order are expected. Indeed, its age is within 400 ± 100 Myr, biased to the solar metallicity (Fig. 4).

The fundamental parameters computed for the 400 Myr solution are: $E(V - I) = 2.29 \pm 0.01$ ($E(B - V) = 1.83 \pm 0.01$ or $A_V = 5.68 \pm 0.02$), $(m - M)_V = 18.6 \pm 0.1$, $(m - M)_O = 12.92 \pm 0.10$, $d_\odot = 3.8 \pm 0.2$ kpc, and $R_{GC} = 4.5 \pm 0.1$ kpc, thus ≈ 2.7 kpc inside the Solar circle. Also, $m_V \approx 13.3$, $m_I \approx 10.7$, $(V - I) = +0.44 \pm 0.03$, $M_V = -5.3 \pm 0.1$ and $M_I = -5.8 \pm 0.1$. Similarly to Teutsch 145, Teutsch 146 can also be considered as an intrinsically bright OC.

4 CLUSTER STRUCTURE

We use the RDPs, defined as the projected stellar number density around the cluster centre to derive structural parameters. Stars with colours unlike those of the cluster CMD morphology are excluded by means of the colour-magnitude filters (shown in Figs. 3 and 4). This procedure enhances the RDP contrast relative to the background, especially in crowded fields (e.g. Bonatto & Bica 2007a; Bonatto & Bica (2007b); Bonatto & Bica (2008b)).

Rings of increasing width with distance from the cluster centre are used to preserve spatial resolution near the centre and minimise noise at large radii. The R coordinate (and uncertainty) of each ring corresponds to the average position and standard deviation of the stars inside the ring. The RDPs of Teutsch 145 and 146 are shown in Fig. 7. The effective (i.e., avoiding border effects) radial range of both RDPs reaches about $4'$, which is clearly less than the cluster size.

To derive cluster structural parameters, we fit the RDPs with the analytical function $\sigma(R) = \sigma_{bg} + \sigma_0 / (1 + (R/R_c)^2)$,

⁴ Derived by means of the Globular Cluster (GC) spatial distribution. Recently, Trippe et al. (2008) found $R_{GC} = 8.07 \pm 0.32$ kpc while Ghez et al. (2008) found $R_{GC} = 8.0 \pm 0.6$ kpc or $R_{GC} = 8.4 \pm 0.4$ kpc, under different assumptions.

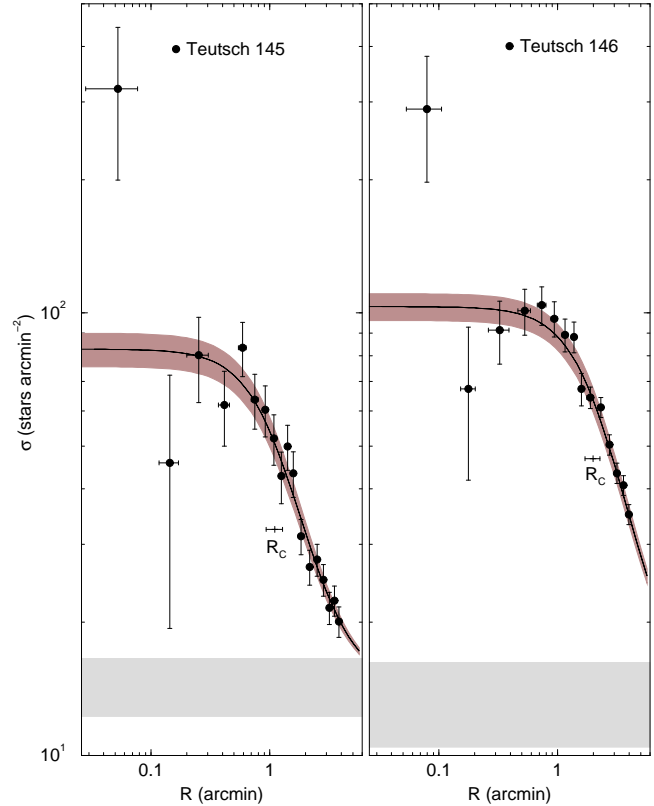


Figure 7. Stellar RDPs built with colour-magnitude filtered photometry together with the best-fit King-like profile (solid line), the 1σ uncertainty and the background level (shaded polygon). Both OCs present a cusp in the innermost RDP bin.

where σ_{bg} is the residual background density, σ_0 is the central density of stars, and R_c is the core radius. Formally, it is similar to the King (1962) function that describes the surface-brightness profiles in the central parts of GCs. However, in the present cases it is applied to star counts, with equivalent results (e.g. Bonatto & Bica 2008a). Given the limited radial range of the RDPs, the background level is little constrained and thus, its fit value has large error bars. Besides, the actual cluster size cannot be precisely determined. The central regions, on the other hand, are well sampled. With the above restrictions in mind, the best-fit solutions (together with the uncertainties) are shown in Fig. 7, and the parameters are given in Table 2.

Within uncertainties, the adopted King-like function describes both RDPs along most of the detected radial range. However, the innermost bin ($R \lesssim 0.1'$) presents a significant excess over the fit in both cases. Such a cusp has been attributed to a post-core collapse structure in old star clusters, like those detected in some GCs (e.g. Trager, King & Djorgovski 1995). Gyr-old OCs, e.g. NGC 3960 (Bonatto & Bica 2006) and LK 10 (Bonatto & Bica 2009a), also present this dynamical evolution-related feature. Thus, the presence of such features in clusters a few 10^8 yrs old located in the inner Galaxy (Sect. 3.2) is not unusual.

Based on the extrapolation of the King-like fit into the background (taking into account the respective uncertainties), we estimate that the cluster radius of Teutsch 145 is

Table 2. Derived structural parameters

Cluster	σ_{bg} (* ' $^{-2}$)	σ_0 (* ' $^{-2}$)	R_c (')	1' (pc)	σ_{bg} (* pc $^{-2}$)	σ_0 (* pc $^{-2}$)	R_c (pc)
(1)	(2)	(3)	(4)	(5)	(6)	(7)	(8)
Teutsch 145	14.4 ± 2.2	68.4 ± 7.2	1.1 ± 0.2	0.774	24.0 ± 3.6	114.2 ± 12.1	0.86 ± 0.13
Teutsch 146	13.3 ± 6.1	90.0 ± 7.2	2.0 ± 0.3	1.113	10.8 ± 5.2	72.6 ± 5.8	2.21 ± 0.31

Table Notes. Col. 5: arcmin to parsec scale.

about $R_{\text{RDP}} \approx 9' \pm 2'$ (≈ 7 pc). For Teutsch 146 we estimate the somewhat larger value $R_{\text{RDP}} \approx 14' \pm 4'$ (≈ 16 pc).

Compared to the core radii derived for a sample of relatively nearby OCs by Piskunov et al. (2007), the King-like values of the present OCs ($0.9 \lesssim R_c(\text{pc}) \lesssim 2.2$) fall around the mean value of that distribution. However, these values should be taken only as representative, since the inner region of both OCs clearly does not follow the King-like profile.

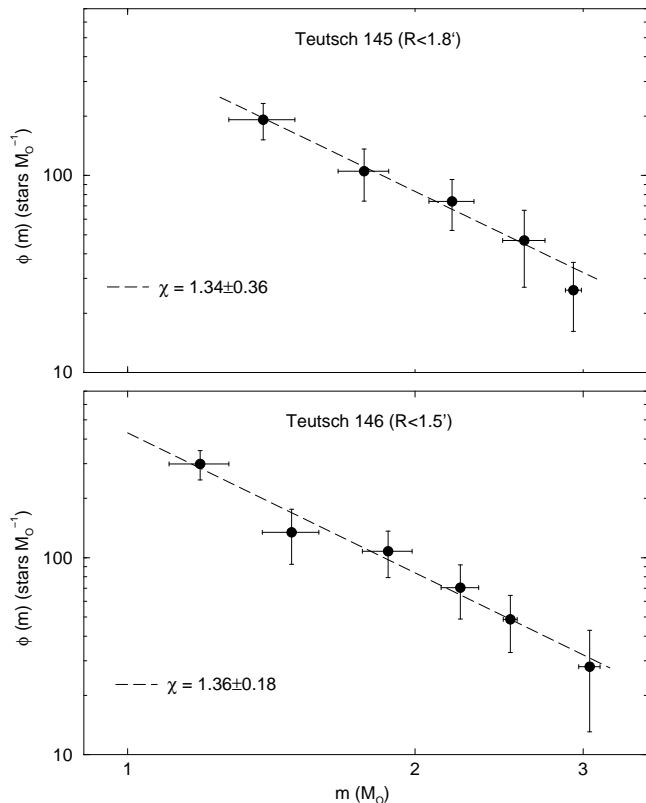
5 MASS ESTIMATE

About 5 mags of the field-decontaminated MS (together with a few giants) of Teutsch 145 and 146 are detected by the GALILEO photometry (Figs. 3-5), which can be used to build the mass function ($\phi(m) = \frac{dN}{dm}$) and estimate the mass stored in stars.

The decontamination algorithm excludes stars in integer numbers from the CMDs, and thus, it should be used essentially to determine the intrinsic CMD morphology. However, when magnitude (or mass) bins are considered, the bin-to-bin subtraction of the comparison field contribution (normalised to the same projected areas) is expected to produce fractional numbers, which should be taken into account by, e.g. the MFs or the cluster mass (e.g. Bonatto & Bica 2005). Thus, the following analyses are based on colour-magnitude filtered photometry (Figs. 3 and 4).

For the present purposes we consider the regions within $R \leq 1.8'$ and $R \leq 1.5'$ (Figs. 1 and 2), respectively for Teutsch 145 and 146, which correspond to ≈ 1.6 pc in both cases. The effective MS stellar mass ranges are $1.17 \leq m(M_\odot) \leq 4.11$ (Teutsch 145) and $0.97 \leq m(M_\odot) \leq 3.17$ (Teutsch 146). The number of member MS and giant stars is derived by counting the stars (in bins of $\Delta V = 0.5$ mag), and subtracting those in the field (normalised to the same area). The corresponding stellar mass in each magnitude bin is taken from the mass-luminosity relation derived from the isochrone fits (Sect. 3.2). We found $m_{\text{MS}} = 397 \pm 37 M_\odot$ and $m_{\text{giant}} = 45 \pm 12 M_\odot$, respectively for the MS and giant stars of Teutsch 145, and the similar values $m_{\text{MS}} = 409 \pm 35 M_\odot$ and $m_{\text{giant}} = 70 \pm 16 M_\odot$ for Teutsch 146. Thus, the respective total stellar mass values inferred within the spatial region considered are $\approx 440 M_\odot$ and $\approx 480 M_\odot$.

With the above data we build the MF for the MSs (Figs. 8). Both MFs are well represented by the function $\phi(m) \propto m^{-(1+\chi)}$, with the slope $\chi = 1.34 \pm 0.36$ and $\chi = 1.36 \pm 0.18$, respectively for Teutsch 145 and 146. These values agree with the $\chi = 1.35$ of Salpeter (1955) initial mass function (IMF). This is not a surprising result, since recent works raise the possibility of a universal initial mass function

**Figure 8.** The intrinsic main-sequence mass functions (black circles) are fitted by the function $\phi(m) \propto m^{-(1+\chi)}$ (dashed line).

that, for the mass range $m \gtrsim 1 M_\odot$, is essentially Salpeter (e.g. Kroupa 2001). Besides, Salpeter-like slopes also occur (for $m \gtrsim 1 M_\odot$) in a variety of OCs younger than about 1 Gyr (e.g. Fig. 12 in Bonatto & Bica 2009b for the near-infrared, and Maciejewski & Niedzielski 2007 in the optical).

Finally, we estimate the total stellar mass (within ≈ 1.6 pc) by extrapolating the observed MFs down to the H-burning mass limit ($0.08 M_\odot$). We assume the universal IMF of Kroupa (2001), which is characterised by the slopes $\chi = 0.3 \pm 0.5$ for the range $0.08 \leq m(M_\odot) \leq 0.5$ and $\chi = 1.3 \pm 0.3$ for $0.5 \leq m(M_\odot) \leq 1.0$. We obtain $m_{\text{extr}} \approx 1400 \pm 500 M_\odot$ in both cases, a value somewhat higher than the mean cluster mass with respect to the nearby OC distribution of Piskunov et al. (2007). For these values, the mass to light ratios are $M/L_V \approx 0.10$ and 0.12 , respectively for Teutsch 145 and 146, consistent with their ages (e.g. Bica, Arimoto & Alloin 1988).

The above mass values should be taken as lower limits,

since the clusters are larger than the region (≈ 1.6 pc) within which the mass functions were computed. Besides, given the restricted spatial range of the observations, the comparison fields are located at the outskirts of the clusters themselves, and thus, an oversubtraction of member stars (mostly low-mass stars) certainly occurred.

6 DISCUSSION

The positions of Teutsch 145 and 146, projected onto the Galactic plane, are given in Fig. 9, which shows the spiral arm structure of the Milky Way based on Momany et al. (2006) and Drimmel & Spergel (2001), derived from HII regions and molecular clouds (e.g. Russeil 2003). The Galactic bar is shown with an orientation of 14° and 6 kpc of total length (Freudenreich 1998; Vallée 2005).

Both OCs are compared with the spatial distribution of the OCs with known age and distance from the Sun given in the WEBDA database. Two age groups are considered, clusters younger and older than 1 Gyr. In the inner Galaxy, dynamical interactions with the disk, the tidal pull of the Galactic bulge, and collisions with giant molecular clouds, tend to destroy OCs, especially the poorly-populated ones, on a timescale of a few 10^8 yr (e.g. Bergond, Leon & Guilbert 2001). In this context, it should be expected to find old OCs preferentially outside the Solar circle (Fig. 9), a region with lowered tidal stress from the Galaxy and with less probability of encounters with giant molecular clouds (e.g. van den Bergh & McLure 1980; Friel 1995; Bonatto & Bica 2007b). A similar scenario, with the outer disk hosting predominantly the old population, has been observed in other galaxies as well, e.g. NGC 300 (Vlajić, Bland-Hawthorn & Freeman 2009). The presence of bright stars in young OCs, on the other hand, allows them to be detected farther than the old ones, especially towards the central Galaxy. Central regions more distant than ≈ 2 kpc begin to be critically affected by completeness effects (due to crowding and high background levels) and enhanced disruption rates (e.g. Bonatto et al. 2006). Besides, all directions show a depletion in the number of OCs detected farther than ≈ 2 kpc.

Teutsch 145, and especially 146, are located close to the Crux-Scutum arm, among the most (centrally) distant OCs so far detected. Since they are projected essentially low on the disk ($|b| \lesssim 0.4^\circ$), tidal stresses related to collisions with the spiral arm may have induced dynamical effects on them (e.g. Gieles, Athanassoula & Portegies-Zwart 2007; Bonatto & Bica 2008b). As discussed in Sect. 4, the central cusp in the RDPs may be an example of such an effect. The preferential low-mass star loss, and the resulting MF flattening, might also reflect this mechanism. However, given the distance of the clusters (Sect. 3.2), the GALILEO photometry could not detect the sub-solar mass range (Sect. 5).

In any case, for both OCs to retain a significant amount of stellar mass (at least $m \sim 1400 M_\odot$) after spending a few 10^8 yrs in the inner Galaxy, their primordial masses might have been significantly higher than the present values.

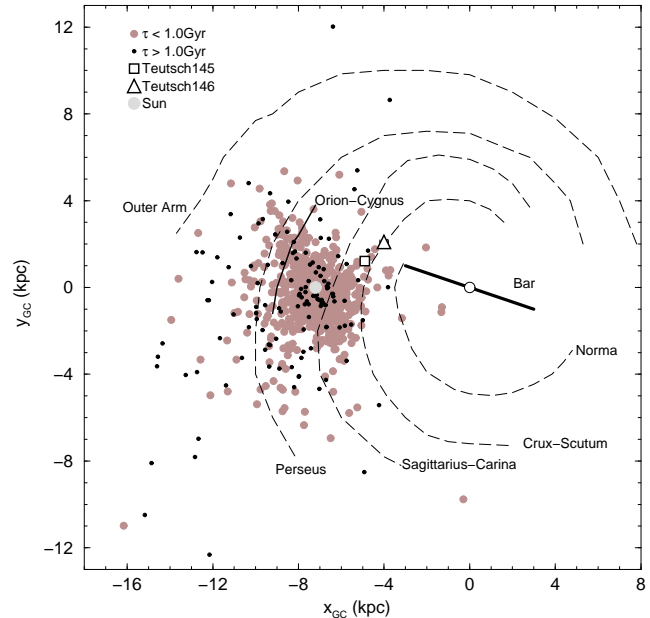


Figure 9. Projected distribution of the present star clusters compared to the WEBDA OCs younger (gray circles) and older than 1 Gyr (black dots). Clusters are shown on a schematic projection of the Galaxy, as seen from the North pole, with 7.2 kpc as the Sun’s distance to the Galactic centre. Main structures are identified.

7 CONCLUDING REMARKS

We use BVI photometry obtained with the TNG (3.58m) telescope to derive astrophysical parameters and investigate the nature of the two optically faint and poorly known OCs Teutsch 145 ($m_V = 12.4$) and Teutsch 146 ($m_V = 13.3$). Located in the 1st Quadrant, both OCs present heavily field-contaminated CMDs, which makes their nature and properties difficult to establish from optical studies in smaller telescopes.

Decontaminated CMDs show that the two clusters exhibit similar properties, basically a well-populated MS together with a few giants. From these we derive ages of 200_{-50}^{+100} Myr and 400 ± 100 Myr, and distances from the Sun $d_\odot = 2.7 \pm 0.3$ kpc and $d_\odot = 3.8 \pm 0.2$ kpc, respectively for Teutsch 145 and 146. Their mass functions, detected for stars more massive than $\approx 1 M_\odot$, present slopes similar to Salpeter’s IMF. Extrapolated to the H-burning limit, both cluster masses are of the order of $1400 M_\odot$, which would characterise them as relatively massive OCs. Intrinsically, they are bright OCs, with integrated $M_V \approx -5.6$ and $M_V \approx -5.3$, respectively. However, given the limited spatial range of the observations, the present-day mass values may be somewhat higher.

Teutsch 145 and 146 are located in the inner Galaxy (more than 2 kpc inside the Solar circle), a region where cluster-disruption processes are important. Besides, they are close to the Crux-Scutum arm. Thus, given the ages, their primordial masses must have been higher than the present-day values. With respect to the radial density distribution of stars, they both present a cusp in the innermost region, which might reflect dynamical effects induced by the important external tidal stresses acting along a few 10^8 yrs. The

present analysis may shed light on issues such as cluster stability, tidal disruption rates and the future cluster evolution in such harsh environment.

ACKNOWLEDGEMENTS

We thank an anonymous referee for interesting suggestions. We acknowledge partial financial support from CNPq (Brazil) and the Ministero dell'Università e della Ricerca Scientifica e Tecnologica (MURST), Italy. This research has made use of the WEBDA database, operated at the Institute for Astronomy of the University of Vienna.

REFERENCES

- Bica E., Arimoto N. & Alloin D. 1988, *A&A*, 202, 8
 Baumgardt H. & Makino J. 2003, *MNRAS*, 340, 227
 van den Bergh S. 1957, *ApJ*, 125, 445
 van den Bergh S. & McLure R.D. 1980, *A&A*, 88, 360
 Bergond G., Leon S. & Guilbert J. 2001, *A&A*, 377, 462
 Bica E., Bonatto C., Barbuy B. & Ortolani S. 2006, *A&A*, 450, 105
 Bica E. & Bonatto C. 2008, *MNRAS*, 384, 1733
 Bica E., Bonatto C. & Camargo D. 2008, *MNRAS*, 385, 349
 Bonatto C. & Bica E. 2005, *A&A*, 437, 483
 Bonatto C., Kerber L.O., Bica E. & Santiago B.X. 2006, *A&A*, 446, 121
 Bonatto C. & Bica E. 2006, *A&A*, 455, 931
 Bonatto C. & Bica E. 2007a, *MNRAS*, 377, 1301
 Bonatto C. & Bica E. 2007b, *A&A*, 473, 445
 Bonatto C. & Bica E. 2008a, *A&A*, 477, 829
 Bonatto C. & Bica E. 2008b, *A&A*, 485, 81
 Bonatto C. & Bica E. 2009a, *MNRAS*, 392, 483
 Bonatto C. & Bica E. 2009b, *MNRAS*, 397, 1915
 Cardelli J.A., Clayton G.C. & Mathis J.S. 1989, *ApJ*, 345, 245
 Drimmel R., & Spergel D.N. 2001, *ApJ*, 556, 181
 Freudenreich H.T. 1998, *ApJ*, 492, 495
 Friel E.D. 1995, *ARA&A* 1995, 33, 381
 Geller A.M., Mathieu R.D., Harris H.C. & McClure R.D. 2009, *AJ*, 137, 3743
 Ghez A.M., Salim S., Weinberg N.N., Lu J.R., Do T., Dunn J.K., Matthews K., Morris M.R. et al. 2008, *ApJ*, 689, 1044
 Gieles M., Athanassoula E. & Portegies-Zwart S.F. 2007, *MNRAS*, 376, 809
 Girardi L., Bertelli G., Bressan A., Chiosi C., Groenewegen M.A.T., Marigo P., Salasnich B. & Weiss A. 2002, *A&A*, 391, 195
 Goodwin S.P. & Bastian N. 2006, *MNRAS*, 373, 752
 von Hoerner S. 1958, *Astrophys.*, 44, 221
 Hole K.T., Geller A.M., Mathieu R.D., Platais I., Meibom S. & Latham D.W. 2009, *AJ*, 138, 159
 Khalisi E., Amaro-Seoane P. & Spurzem R. 2007, *MNRAS*, 374, 703
 King I. 1962, *AJ*, 67, 471
 Kronberger M., Teutsch P., Alessi B., Steine M., Ferrero L., Graczevski K., Juchert M., Patchick D. et al. 2006, *A&A*, 447, 921
 Kroupa P. 2001, *MNRAS*, 322, 231
 Lamers H.J.G.L.M. & Gieles M. 2006, *A&AL*, 455, 17
 Lata S., Pandey A.K., Sagar R. & Mohan V. 2002, *A&A*, 388, 158
 Maciejewski G. & Niedzielski A. 2007, *A&A*, 467, 1065
 Momany Y., Zaggia S., Gilmore G., Piotto G., Carraro G., Bedin L.R. & de Angeli F. 2006, *A&A*, 451, 515
 O'Donnell J.E. 1994, *ApJ*, 422, 1580
 Oort J.H. 1958, in *Ricerche Astronomiche*, 5, 415, Specola Vaticana, Proc. of a Conference at Vatican Observatory, Castel Gandolfo, May 20-28, 1957, ed. D.J.K. O'Connell
 Ortolani S., Bonatto, C., Bica E. & Barbuy B. 2009, *AJ*, 138, 889
 Piskunov A.E., Schilbach E., Kharchenko N.V., Röser S. & Scholz R.-D. 2007, *A&A*, 468, 151
 Russeil D. 2003, *A&A*, 397, 133
 Salpeter E. 1955, *ApJ*, 121, 161
 Schlegel D.J., Finkbeiner D.P. & Davis M. 1998, *ApJ*, 500, 525
 Skrutskie M., Schneider S.E., Stiening R., Strom S.E., Weinberg M.D., Beichman C., Chester T., Cutri R. et al. 1997, in *The Impact of Large Scale Near-IR Sky Surveys*, ed. F. Garzon et al., Kluwer (Netherlands), 210, 187
 Spitzer L. 1958, *ApJ* 127, 17
 Trager S.C., King I.R. & Djorgovski S. 1995, *AJ*, 109, 218
 Trippe S., Gillessen S., Gerhard O.E., Bartko H., Fritz T.K., Maness H.L. Eisenhauer F., Martins F., et al. 2008, *A&A*, 492, 419
 Vallée J.P. 2005, *AJ*, 130, 56
 Vlajić M., Bland-Hawthorn J. & Freeman K.C. 2009, *ApJ*, 697, 361

